Mineral alteration of a Type B CAI from the reduced CV3 chondrite, Efremovka.

Y. Enokido, T. J. Fagan, H. Aragane, Department of Earth Sciences, Waseda University, Tokyo, Japan. (eno373@moegi.waseda.jp)

Introduction:

Ca-Al-rich inclusions (CAIs) from CV chondrites have been used to determine the age of the solar system and to interpret high-temperature processes of the inner solar system [1,2]. Many CAI studies have focused on the CV3 Allende; however, recent work shows that Allende has undergone metamorphism in its parent body, and thus nebular effects may be difficult to disentangle from parent body effects [3-5]. Reduced CV chondrites, such as Efremovka, have not undergone the same extent of metamorphism as Allende [4], suggesting that nebular effects would be easier to identify in Efremovka. However, Efremovka has also undergone some metamorphism. In this study, we focus on mineralogy and textures in one type B1 CAI (CGI-10) from Efremovka, and find that secondary minerals—though not as abundant as in Allende CAIs—occur in CGI-10 and secondary effects should be considered during studies of Efremovka CAIs.

Methods:

Minerals and textures were characterized using a petrographic microscope, back-scattered electron (BSE) images and elemental X-ray maps. Elemental maps, BSE images and quantitative analyses of minerals were collected using a JEOL JXA-8900 electron probe micro-analyzer (EPMA) at Waseda University (WU). Additional BSE and cathodoluminescence (CL) images were collected using a S-3400N Hitachi scanning electron microscope (SEM) with a Gatan Mono-CL4 detector at WU.

Determining the mode of minerals in CGI-10 was hindered by the abundance of fine-grained spinel in this CAI (Figs. 1,2). Therefore, nine sets of elemental maps were collected at high spatial resolution (2 μm) and then combined in a mosaic. The mosaic was overlain by a grid using Adobe Illustrator, and then the mineral at each grid node was identified based on elemental abundances. Even at the high spatial resolution of our elemental maps, many grid nodes fell on grain boundaries of spinel and adjacent minerals. We counted these nodes as half spinel, half other mineral. All grid points were counted by the lead author (YE) with at least one other person, including the co-authors and WU students Y. Yoshida, R. Aoki and H. Fukushima.

Then we compare CGI-10 with Allende CAIs (3655A, 3529-47, 4022) described previously [5,6]. MicroRaman analyses of $CaAl_2Si_2O_8$ phases in 3655A and CGI-10 were attempted in collaboration with S. Takabe, of Prof. Ogasawara laboratory (WU). Primary anorthite and secondary dmisteinbergite were successfully identified in 3655A and 3529-47, but, the spectra from CGI-10 were completely masked by fluorescence.

Results:

The CAI modes show that secondary minerals are much less abundant in CGI-10 (from Efremovka) than in the Allende CAIs; however, secondary nepheline, sodalite and a Ca-Al-rich elongate secondary mineral (ESM) occur in Efremovka (Table 1). Secondary minerals in CGI-10 are concentrated near the margin of the CAI, as shown by the CAI Na Kα map (Fig. 1). This alkali-rich domain is similar to the alkali-FeO-rich alteration that occurs near the rims of Allende CAIs [5]. On the other hand, the grossular-rich veins (with monticellite, wollastonite) that occur in the interiors of type B CAIs in Allende were not observed in CGI-10.

ESM with composition ~$CaAl_2Si_2O_8$ occurs in the near-rim alkali-FeO-rich alteration domains in Allende CAIs and in one locality in CGI-10 (Fig. 2). TEM results from Allende CAIs 3529-47 and 4022 show that the dominant ESM polymorph is dmisteinbergite, though some anorthite was also identified in 3529-47 [6]. In both CAIs, crystals of $CaAl_2Si_2O_8$ are intercalated with thin lamellae of biopyribole [6]. Our Raman analyses show that the ESM in CAI 3655A also consists of dmisteinbergite. Dmisteinbergite occurs in similar textural settings in the CV3 chondrite NWA 2086 [7]. In contrast, the ESM in CGI-10 is probably dominated by the anorthite polymorph, because it has bright CL similar to the CL of primary anorthite in type B CAIs (Fig. 2).

The absence of grossular-rich veins in CGI-10 indicates a lower extent of mineral alteration in CGI-10 in comparison to Allende CAIs [8]. However, nepheline and sodalite replace melilite near the rims of CGI-10 and Allende CAIs, indicating that metasomatic conditions in both Allende and Efremovka resulted in transport of alkalis and Cl into CAIs, where melilite broke down to form feldspathoids ±ESM. Similarities in mineral alteration of all chondrite components (e.g., fayalitic olivine-rich rims on forsterite in chondrules, AOAs and matrix grains in Allende) suggest that mineral replacement took place after chondrite components were assembled together during parent body metamorphism [3].

The lower extent of replacement in CGI-10 may be due to lower metamorphic temperature [4] and/or the lower porosity [8] of Efremovka. The lower porosity of Efremovka may have resulted from intense shock metamorphism during an early-stage impact event on the Efremovka parent body [9]. The occurrence of anorthite as ESM in CGI-10 vs. mostly dmisteinbergite in the Allende CAIs probably reflects kinetics of crystal growth during fluid-assisted metamorphism [6]. In any case, our results show that CGI-10 has undergone some metasomatic alteration. Thus, parent body effects should be considered when Efremovka CAIs are used to interpret nebular processes.

References: [1] Grossman L. (1975) GCA 39, 433-454. [2] MacPherson G.J. (2005) in Treatise in Geochemistry 1 (A. M. Davis, editor), p. 201-268. [3] Krot A.N. et al. (1998) MaPS 33, 1065-1085. [4] Bonal L. et al. (2006) *GCA, 70,* 1849-1863. [5] Fagan T.J. et al. (2007) MaPS 42, p. 1221-1240. [6] Brearley A.J. et al. (2014) LPSC #2287. [7] Fintor K. et al (2014) MaPS 49, 812-823. [8] MacPherson G.J. and Krot A.N. (2014) MaPS 49, 1250-1270. [9] Macke R.J. et al. (2011) MaPS 46, 1842-1862

Table 1. Modes of CAIs from Efremovka, Allende (vol.%).

	Efremovka	Allende		
CAI (type):	CGI-10 (B1)	3655A (B1)	4022 (B2)	3529-47 (FTA)
melilite	45.9	29.6	27.3	15.4
fassaite	16.5	24.1	21.5	0.15
anorthite	20.4	3.9	7.5	0
spinel	15.3	23.8	12.1	4.5
hibonite	0	0.1	0	0
diopside	0	0	0.4	18.1
perovskite	0.1	0	0	0.61
primary	***98.2***	***79.8***	***68.9***	***38.7***
grossular	0	12	18.9	12.5
monticellite	0	4.4	3.3	0
wollastonite	0	0.9	0.5	0
ESM*	tr	0.6	2.5	21.5
Fe-spinel	0.2	0.5	2.5	0
sodalite	0.9	0.1	0.8	1.52
nepheline	0.5	0.1	1.6	5.66
high Ca-pyx	0.1	0	0.6	0
secondary	***1.6***	***18.6***	***30.6***	***41.2***
unknown	0.1	0	0.6	2.23
total points	2143	1536	1063	1031

*ESM = elongate secondary mineral; tr = trace amount.

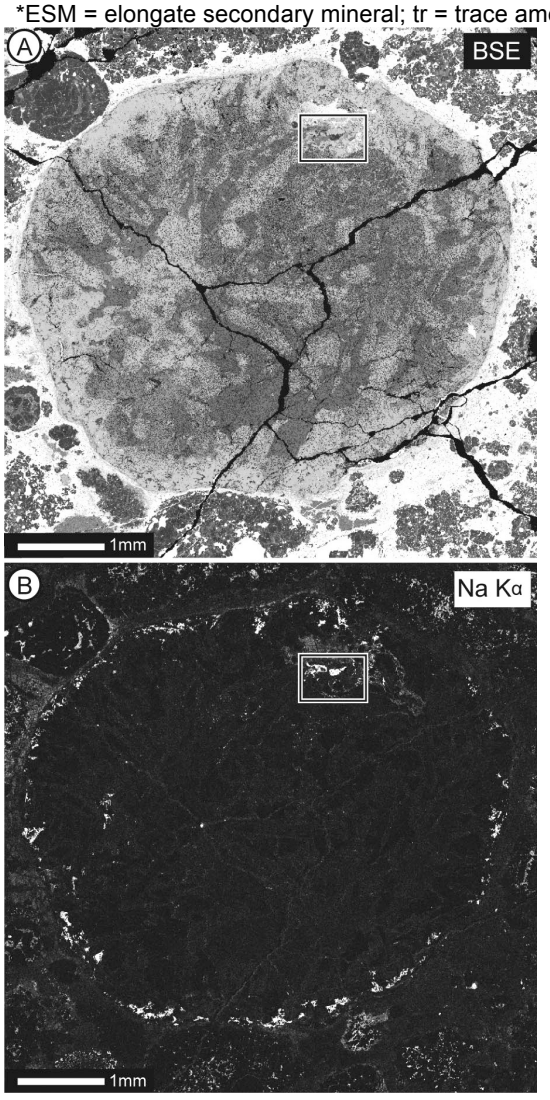

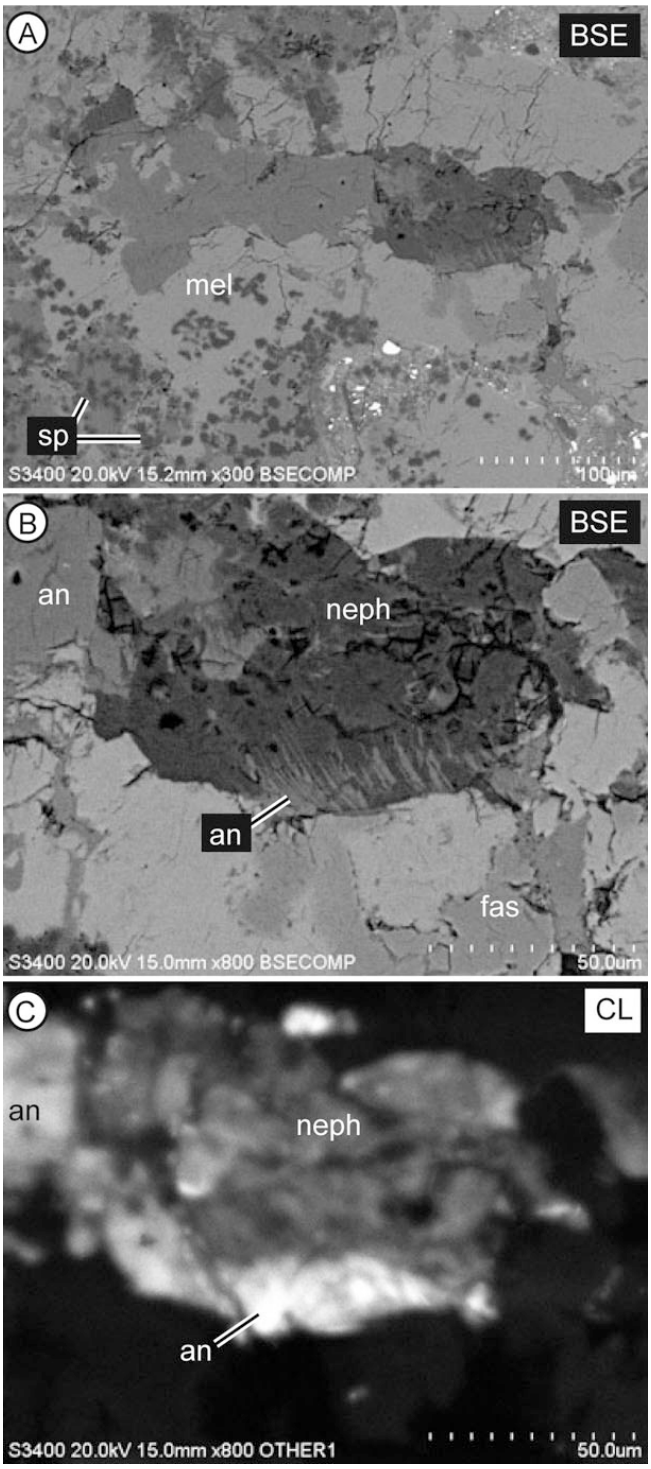

Fig. 2. BSE (A,B) and cathodoluminescence (C) images of an altered domain in CGI-10. The coarse, tabular texture of the anorthite crystal at upper left of (B) and (C) is characteristic of primary anorthite, in contrast to the fine, feathery texture of secondary anorthite intercalated with nepheline. Mineral abbreviations: an = anorthite; fas = fassaite; mel = melilite; neph = nepheline ; sp = spinel.

← Fig. 1. BSE and Na Kα maps of Efremovka CAI CGI-10. Tiny dark spots in (A) are fine grains of Mg-spinel (see Fig. 2A). Boxed area is shown at higher magnification in Fig. 2.